Lasers in Manufacturing Conference 2019

Generation of internal 3D microfluidic architectures in polymers by fs laser processing

Gian-Luca Roth[a*], Bastian Wolf[a], Cemal Esen[b], Ralf Hellmann[a]

[a]*Applied Laser and Photonics Group, University of Applied Sciences Aschaffenburg, Würzburger Str. 45, 63739 Aschaffenburg, Germany*
[b]*Applied Laser Technologies, Ruhr-University Bochum, Universitätsstr. 150, 44801 Bochum, Germany*

Abstract

Microfluidic lab on chip systems require components to transport, mix, separate and analyse small volumes of different fluids. In this study, we report on the laser generation of internal hollow architectures created by focused 514 nm femtosecond laser pulses inside PMMA bulk material. Size and cross-sectional shape of a single internal generated microchannel are determined by the intensity distribution inside the focal voxel and can be controlled either by the numerical aperture of the focusing objective or by laser beam shaping. As both approaches are practically limited with respect to the realizable cross-sectional shapes, we present a process based on an internal hatching to expand the achievable channel cross-sections and thereby enable the possibility to create complex 3D shaped internal structures. This process is applied to create fully internal functional microfluidic elements such as mixers which are part of most polymer lab-on-chip systems.

Keywords: laser materials processing; polymer; ultrashort pulse; microfluidics; hollow microchannels

1. Introduction

Lab-on-chip (LOC) devices are able to deliver efficient micro-total analysis in basic research and are under development towards the application as medical and diagnostic devices [Luka, 2015; Trautmann, 2019]. The main component of common LOC devices is a microfluidic architecture to transport and manipulate a reagent [Sackmann, 2014]. The possibilities on the design of such a microfluidic layout are mainly given by the fabrication technology [Cheng, 2017]. As State-of-the-art devices are made of transparent substrate materials such as glass [Al-Halhouli, 2018] or polymers [Volpe, 2019; Hessler, 2017] fabrication technologies

* Corresponding author. Tel.: +49 6021 81 3616 .
E-mail address: gian-luca.roth@th-ab.de .

include different photolithographic approaches, hot embossing or casting processes, respectively. However, all of these processes can be characterized as to be limited 2 or 2.5D surface processes which do not allow a direct fabrication of internal multilevel microfluidic architectures. A possibility to overcome this limitation is the usage of femtosecond laser pulses. Ultrashort pulse lasers are widespread in use in the processing of transparent materials such as in ablation processes [Schwarz, 2018], surface nanostructuring [Schwarz, 2017] or welding [Roth, 2016]. Furthermore, femtosecond laser processing is not limited to an absorbing layer or surface and can thereby be used to create internal material modifications inside of transparent materials [Gattass, 2008]. These modifications can either be used as optical elements such as waveguides [Martinez Vazquez, 2009] or can be selectively removed i.e. using a suitable etchant [Sugioka, 2012] or a heat treatment of the sample [Roth, 2017] depending on the substrate material.

Femtosecond laser processing inside of transparent materials such as glass or polymers is limited due to the small 3D voxels of the corresponding microscope objectives to maximum feature sizes with cross-sections of several hundreds of square micrometers [Roth, 2018]. Using an elliptical input beam the cross-section of the focal voxel can be effectively adjusted as shown by [Diez-Blanco, 2007; Roth, 2019] however, these approaches are practically restricted with respect to the achievable modification size. Thus, processes like selective laser etching are usually based on a hatching process to achieve larger irradiated areas and thereby larger internal feature sizes [Ho, 2012; Paiè, 2014; Weingarten, 2017; Sima, 2018].

In this contribution, we report on the creation of internal microfluidic structures and chambers in PMMA by using a hatching process. Size, quality and overall appearance of corresponding internal structures are mainly defined by the overall irradiation dose of a single channel as well as the vertical and horizontal distance between single hatching lines. Therefore, we carefully study the impact of different irradiation dose on the laser generation process by creating single microchannels which are used to be the starting point of the development of the hatching process. The application of the process to generate functional microfluidic structures is demonstrate by creating and using an internal mixer layout.

2. Experimental

2.1. Laser system

We used an ultrashort pulse laser (Light Conversion, Pharos-10-600) with a fundamental wavelength of 1028 nm having an adjustable pulse duration from 220 fs to 15 ps and variable repetition rate up to 610 kHz. By using a second harmonic generation module, a laser wavelength of 514 nm can be emitted. The laser beam is focused by an air objective with a NA of 0.5 (Zeiss, EC Epiplan-Neofluar). Samples are positioned using translation stages with an accuracy of 250 nm (Aerotech, ANT130-XY) and a repeatability of 75 nm. The vertical focal position is controlled by a nanopositioning z-stage (Aerotech, ANT95-50-L-Z). An on-axis CCD-camera (Imagingsource, DMK 27AUJ003) is used to align the setup and to monitor the shaped beam profile.

2.2. Materials

Commercially available bulk PMMA sheets (type ME303010) with a thickness of 1.1 mm are used in this study. A CO_2 Laser is applied to cut the sheets into size of 20 x 20 mm and 15 x 40 mm for the specimens. The polymer exhibits a glass transition temperature of 105 °C. The refractive index *n* of the material at the laser wavelength of 514 nm is 1.4943 at room temperature calculated by Sellmeier equation.

2.3. Methods and Characterization

Laser direct generation of microchannels consists of two process steps. Firstly, the specimens are irradiated by focused femtosecond pulses triggering a nonlinear absorption inside the focal volume. Definable 3D geometries can be created by translating the focal spot in three dimensions inside the bulk. Secondly, the specimens are placed on a hot plate between two glass substrate and are annealed at 200 °C for 60 seconds from each side. It is worthwhile to note, that prior annealing no microchannels are found, i.e. their formation is clearly linked to the annealing process. Further details on the channel formation process are given in [Roth, 2017].

In order to characterize microchannel cross-sections, the treated specimens are ground down to the created structures and polished. An ultrasonic bath is used to remove debris from this process step. Channel geometries are measured by using reflection and transmission light microscopes (Nikon, 70 Eclipse LVDIA-N; Leica, DVM6).

3. Results and Discussion

3.1. Characterization of the beam propagation

The coaxial CCD cam is used to monitor the beam profile reflected from the backside of the PMMA chips. By employing a suitable wavefront correction of the incoming laser beam, spherical aberration effects can be effectively avoided. The beam profile in propagation direction (X-Z & Y-Z-cross-section) is measured using a z-stacking of single beam profiles captured with a step size of 250 nm and is depicted in Fig. 1 b and c.

The width of the focal spot in x and y direction is given by the focusing conditions of both axes. By the application of an elliptical input beam (ellipticity: 15, formed by a slit aperture) the effective NA on the major axis is way higher than on the minor axis. This results in different focal widths as depicted in Fig.1 a and introduces a preferred writing direction. Focal spot dimensions compromise a length of 24 µm and a width of 1.5 µm (both measured at $1/e^2$). The focal voxel itself can be described as an upright standing thin disk which is stretched by a factor of 1.49 due to the refractive index of the PMMA chip and is designed to create internal microchannels with an aspect ratio between 1.2 and 1.4 depending on further process parameters and using the preferred writing direction perpendicular to the minor axis of the input beam.

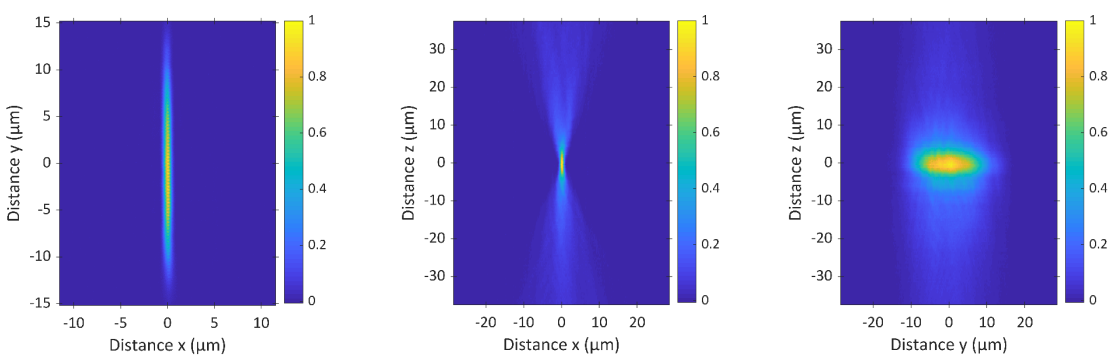

(a) (b) (c)

Fig. 1. Measured normalized beam profile of the elliptical focal voxel in X-Y cross-section at the focal position (a), X-Z-cross-section (b) and Y Z cross-section(c) using an ellipticity of 15 and an effective NA of 0.24 on the major axis.

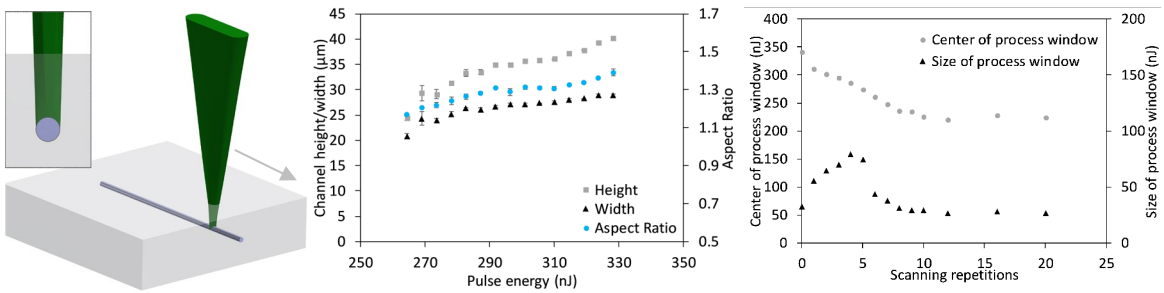

Fig. 2. Scheme of the generation of a single microchannel using an elliptical beam profile (a), influence of the laser pulse energy on the microchannel dimensions using 2 scanning repetitions (b), influence of the size and location of process window for the usable laser pulse energy based on the scanning repetitions (c).

3.2. Influence of laser pulse energy and scanning repetitions on resulting single line microchannels

The overall geometry of a fs laser generated internal microchannel is generally defined by the applied focusing condition on the major and minor axis. Studies regarding the evolution of the channel profile using different focusing conditions are shown in one of our previous publications [Roth, 2019]. However, the irradiation dose i.e. the energy per pulse and the number of pulses per point can be used to trim height, width and aspect ratio of a microchannel or to define the process window. In this study, we select a constant pulse to pulse distance of 600 nm which corresponds to a pulse overlap of 60 % assuming a focal width of 1.5 µm. Thus, a variation of the irradiation dose is achieved by a variation of the laser pulse energy and the number of scanning repetitions. Further constant process parameters in this study are the laser wavelength of 514 nm, a laser pulse duration of 450 fs, a pulse repetition rate of 25 kHz, a scanning speed of 15 mm/s, a writing depth of 500 µm including a suitable correction of spherical aberration effects, an input beam ellipticity of 15 and a numerical aperture NA of 0.24 on the major axis, respectively.

Height, width and aspect ratio of microchannels generated using different laser pulse energies are depicted in Fig. 2 b. It is clearly visible, that using higher laser pulse energies leads to increased size of the microchannel. Due to the beam size development in propagation direction, the channel height is increasing slightly faster than the channel width which results in a higher aspect ratio of the microchannel geometry using higher pulse energies. The process window to generate homogenous microchannels is limited on the lower side by a irradiation which is insufficient for a microchannel generation and by a distorted channel cross-section with an arrow head like shape which is obtained on the upper side [Del Hoyo, 2015].

With respect to the line and pulse overlap which will affect the total irradiation dose using a hatching process, we study the effect of the number of scanning repetitions on the process window. In Fig. 1 c size and location of the process window for the parameter laser pulse energy is given for different numbers of scanning repetitions. The process window as well as its location correspond directly to the number of scanning repetitions. Using a higher number of scanning repetitions, a lower laser power is necessary to achieve a microchannel formation. Furthermore, the upper limited of the process window is given by a refocusing effect for lower number of scanning repetitions and an oversaturated exposing dose using a higher number of scanning repetitions. The refocusing effect is observed for a laser pulse energy above 360 nJ in a single pass process design.

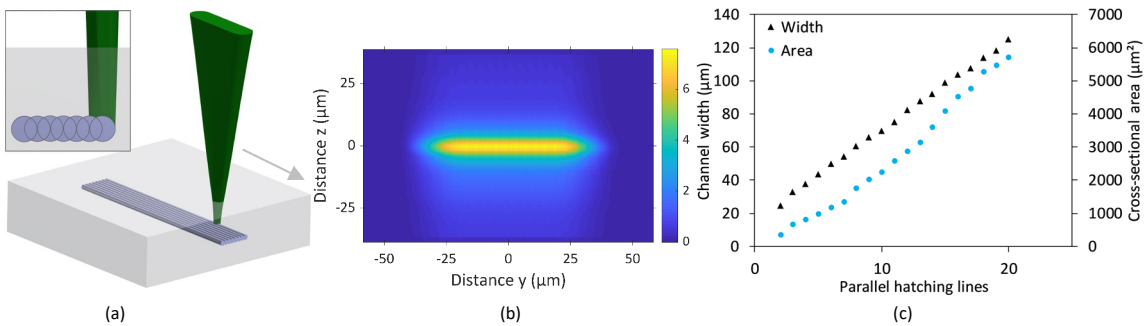

Fig. 3. Schema of the horizontal hatching process using an elliptical beam profile (a), cross-section of the irradiation profile using a hatching distance of 4 µm based on the measured beam profile in Fig. 1 (c) (b), influence of the number of parallel horizontal hatching lines on the channel width (c).

3.3. Generation of internal hatched structures

To generate reproducible internal hatched structures, a homogenous irradiation profile is required. The number of scanning repetitions is set to zero and the irradiation dose is adjusted by the laser pulse energy to achieve a reproducible and homogenous channel formation at the given hatch distance. The quality of the hatched structures is monitored using the waviness of the walls perpendicular to the hatching orientation. The hatching itself is performed in a horizontal and vertical direction to achieve both, flat oriented (Fig. 3 a) and upright standing (Fig. 4 a) chambers. Corresponding irradiation profiles are given in Fig. 3 b and Fig. 4 b which are calculated based on the measured beam profile in propagation direction as depicted in Fig. 1. The hatching distance is set to 4 µm in horizontal direction and 2 µm in vertical direction to achieve homogenous profiles. The accumulated fluency is by a factor of 7.5 and 11.6, respectively, larger than compared to writing a single line using a single pass process. The size of the hatched microchannels can be easily controlled and adjusted by the number of parallel lines in y- or z-direction. In Fig 3 c, width and volume of a horizontally hatched microchannel are given. Channels are created using only a single pass, a writing speed of 15 mm/s and 290 nJ in horizontal hatching respectively 260 nJ in a vertical orientated hatching.

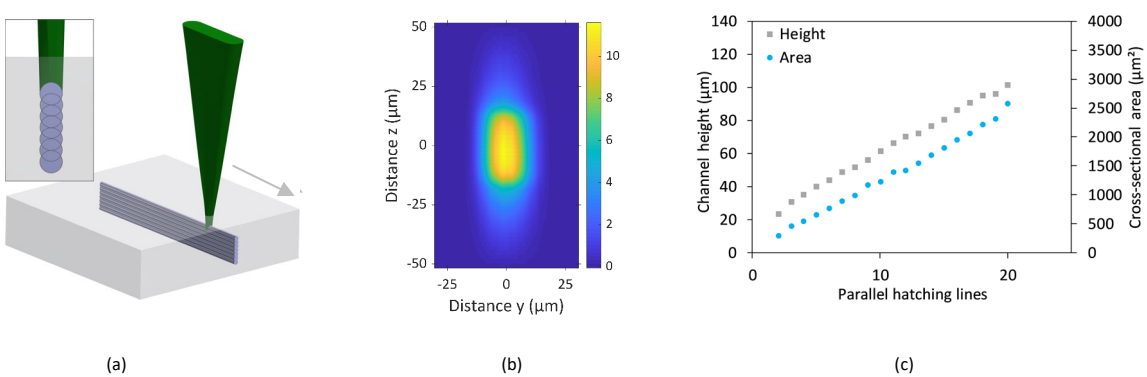

Fig. 4. Schema of the vertical hatching process using an elliptical beam profile (a), cross-section of the irradiation profile using a hatching distance of 2 µm based on the measured beam profile in Fig. 1 (c) (b), influence of the number of parallel vertical hatching lines on the channel height (c).

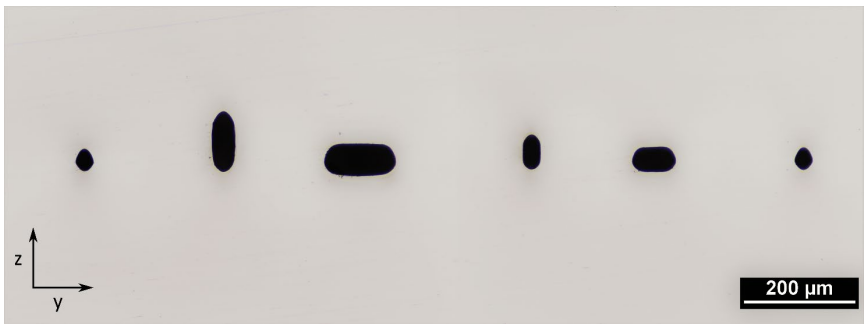

Fig. 5. Cross-section of microchannels generated with different irradiation patterns using a single line, 10 parallel lines and 20 parallel lines in horizontal and vertical direction, respectively. Microchannels appear black due to the transmission light microscopy.

It is clearly visible, that the width is directly proportional to the irradiated area. However, the height of the generated structure is also slightly affected by the number of parallel lines, therefore the cross-sectional area increases super proportional. This effect is contributed to the internal pressure during the annealing process which results in an expansion of the gaseous degenerated PMMA into the softened polymer around the irradiated area. In accordance to this, a comparable effect is also observed using a vertical hatching, shown in Fig. 4 c.

Cross-sections of single microchannel as well as horizontally and vertically hatched structures with a length of 10 mm are given in Fig. 5. The walls of the channels are smooth and well defined without any irregular patterning or a surface waviness based on the hatching process. The origin shape of the single irradiation profile determines the form of the end face of the hatched structure. The hatching distance stayed constant at 4 µm in horizontal direction and 2 µm in vertical direction.

3.4. Application of the hatching process to generate internal microfluidic architectures

The presented hatching process is used to produce an internal microfluidic structure in a single production step. The designed structure is shown in Fig. 6 and consists of a microchannel architecture with a width of 88 µm and a height of 41 µm and is created in a depth of 500 µm. The channel is generated using 11 parallel lines or a corresponding writing length and is hatched bi-directionally at a constant hatching angle. The structure has a maximal channel length of 75 mm. The microfluidic structure consists of 20 turns to ensure a sufficient mixing of the input fluids. Microfluidic connection ports appear as dark spots in Fig. 6. The ports are drilled using a femtosecond laser ablation process employing the same laser source as used for the channel generation but in combination with a galvanometer scanner and a NA of 0.018. A comparable approach has already been demonstrated by [Hessler, 2017].

The functionality of the microfluidic chip is tested in a microfluidic setup using different colored deionized water. The flow rates of both liquids are controlled by two external microfluidic pumps. Input ports are on the left side of the chip (Fig. 6). After the Y-shaped combiner fluids do not mix due to the laminar stream inside the microchannel and flow side by side. By including turns into the microfluidic layout, the diffusion mixing is enhanced by the introduction of perturbations into the laminar flow. At the end of the mixing device (right side of the chip) both liquids are successfully mixed.

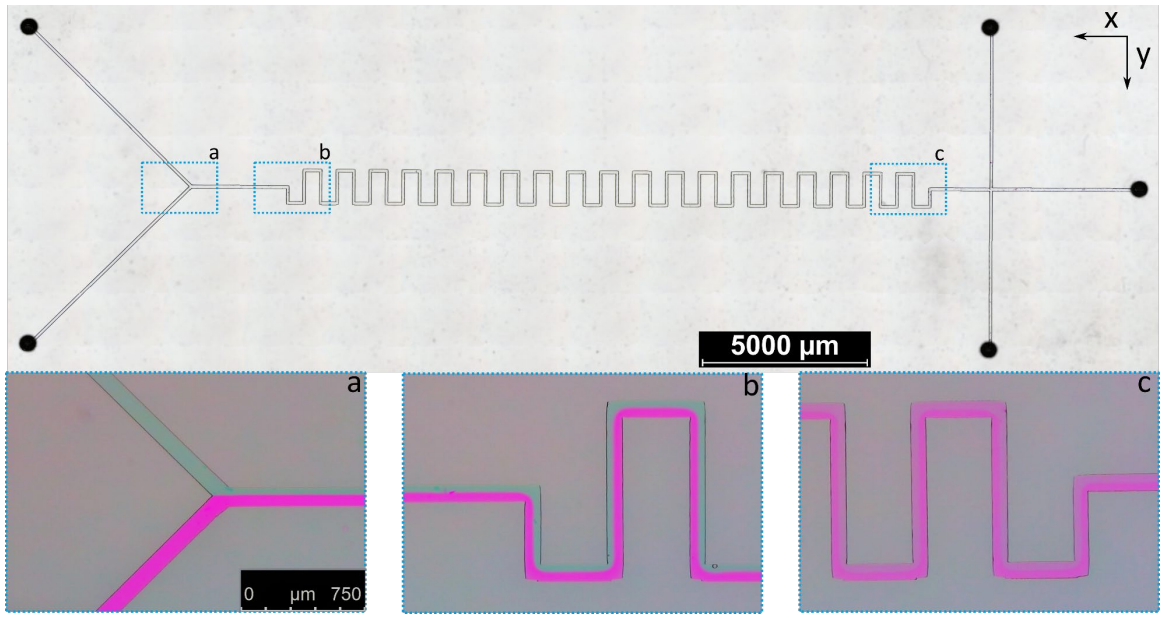

Fig. 6. Top View on the generated internal microfluidic mixer structure. Insets are microscope pictures taken during the microfluidic characterization at different positions of the structure.

4. Conclusion

In this contribution, femtosecond laser generation of internally hatched microfluidic structures is studied. The influence of the irradiation dose on the channel formation is analyzed and transferred to a hatching process. Based on a regular intensity distribution, homogenous and smooth internal channels are creatable. By using a suitable hatching orientation, height and width of an internal microchannel can be directly varied and controlled by the number of parallel hatching lines. Generated structures are used in a microfluidic testing setup and demonstrated as a functional mixing device. The presented results expand the usability of the femtosecond laser generation of internal microchannels and will foster the development of 3D polymer LOC devices using ultra short laser pulses.

References

Al-Halhouli, A., Al-Faqheri, W., Alhamarneh, B., Hecht, L., Dietzel, A. 2018. Spiral Microchannels with Trapezoidal Cross Section Fabricated by Femtosecond Laser Ablation in Glass for the Inertial Separation of Microparticles, Micromachines 9,

Cheng, Y. 2017. Internal Laser Writing of High-Aspect-Ratio Microfluidic Structures in Silicate Glasses for Lab-on-a-Chip Applications, Micromachines 8, p. 59.

Del Hoyo, J., La Cruz, A. R. de, Grace, E., Ferrer, A., Siegel, J., Pasquazi, A., Assanto, G., Solis, J. 2015. Rapid assessment of nonlinear optical propagation effects in dielectrics, Scientific Reports 5, p. 7650.

Diez-Blanco, V., Siegel, J., Ferrer, A., La Ruiz de Cruz, A., Solis, J. 2007. Deep subsurface waveguides with circular cross section produced by femtosecond laser writing, Applied Physics Letters 91, p. 51104.

Gattass, R. R., Mazur, E. 2008. Femtosecond laser micromachining in transparent materials, Nature photonics 2, p. 219.

Hessler, S., Rüth, M., Sauvant, C., Lemke, H.-D., Schmauss, B., Hellmann, R. 2017. Hemocompatibility of EpoCore/EpoClad photoresists on COC substrate for optofluidic integrated Bragg sensors, Sensors and Actuators B: Chemical 239, p. 916.

Ho, S., Herman, P. R., Aitchison, J. S. 2012. Single- and multi-scan femtosecond laser writing for selective chemical etching of cross section patternable glass micro-channels, Applied Physics A 106, p. 5.

Luka, G., Ahmadi, A., Najjaran, H., Alocilja, E., DeRosa, M., Wolthers, K., Malki, A., Aziz, H., Althani, A., Hoorfar, M. 2015. Microfluidics Integrated Biosensors: A Leading Technology towards Lab-on-a-Chip and Sensing Applications, Sensors 15, p. 30011.

Martinez Vazquez, R., Osellame, R., Cretich, M., Chiari, M., Dongre, C., Hoekstra, H. J. W. M., Pollnau, M., van den Vlekkert, H., Ramponi, R., Cerullo, G. 2009. Optical sensing in microfluidic lab-on-a-chip by femtosecond-laser-written waveguides, Analytical and bioanalytical chemistry 393, p. 1209.

Paiè, P., Bragheri, F., Vazquez, R. M., Osellame, R. 2014. Straightforward 3D hydrodynamic focusing in femtosecond laser fabricated microfluidic channels, Lab on a Chip 14, p. 1826.

Roth, G.-L., Esen, C., Hellmann, R. 2017. Femtosecond laser direct generation of 3D-microfluidic channels inside bulk PMMA, Optics Express 25, p. 18442.

Roth, G.-L., Esen, C., Hellmann, R. 2019. Circular microchannels inside bulk polymethylmethacrylate generated by femtosecond laser using slit beam shaping, Journal of Laser Applications 31, p. 22603.

Roth, G.-L., Esen, C., Hellmann, R. 2018. Control of femtosecond laser generated microfluidic channels inside poly(methyl methacrylate), Journal of Laser Applications 30, p. 32016.

Roth, G.-L., Rung, S., Hellmann, R. 2016. Welding of transparent polymers using femtosecond laser, Applied Physics A 122, p. 1.

Sackmann, E. K., Fulton, A. L., Beebe, D. J. 2014. The present and future role of microfluidics in biomedical research, Nature 507, p. 181.

Schwarz, S., Rung, S., Esen, C., Hellmann, R. 2018. Fabrication of a high-quality axicon by femtosecond laser ablation and CO 2 laser polishing for quasi-Bessel beam generation, Optics Express 26, p. 23287.

Schwarz, S., Rung, S., Hellmann, R. 2017. One-dimensional low spatial frequency LIPSS with rotating orientation on fused silica, Applied Surface Science 411, p. 113.

Sima, F., Sugioka, K., Vázquez, R. M., Osellame, R., Kelemen, L., Ormos, P. 2018. Three-dimensional femtosecond laser processing for lab-on-a-chip applications, Nanophotonics 7, p. 613.

Sugioka, K., Cheng, Y. 2012. Femtosecond laser processing for optofluidic fabrication, Lab on a Chip 12, p. 3576.

Trautmann, A., Roth, G.-L., Nujiqi, B., Walther, T., Hellmann, R. 2019. Towards a versatile point-of-care system combining femtosecond laser generated microfluidic channels and direct laser written microneedle arrays, Microsystems & Nanoengineering 5, p. 6.

Volpe, A., Paiè, P., Ancona, A., Osellame, R. 2019. Polymeric fully inertial lab-on-a-chip with enhanced-throughput sorting capabilities, Microfluidics and Nanofluidics 23, p. 37.

Weingarten, C., Steenhusen, S., Hermans, M., Willenborg, E., Schleifenbaum, J. H. 2017. Laser polishing and 2PP structuring of inside microfluidic channels in fused silica, Microfluidics and Nanofluidics 21, p. 165.